Applied Catalysis B: Environmental 303 (2022) 120893

Contents lists available at ScienceDirect

Applied Catalysis B: Environmental

journal homepage: www.elsevier.com/locate/apcatb

Coupling Ni-substituted polyoxometalate catalysts with water-soluble CdSe quantum dots for ultraefficient photogeneration of hydrogen under visible light

Mo Zhang, Xing Xin, Yeqin Feng, Junhao Zhang, Hongjin Lv *, Guo-Yu Yang *

MOE Key Laboratory of Cluster Science, Beijing Key Laboratory of Photoelectroic/Electrophotonic Conversion Materials, School of Chemistry and Chemical Engineering, Beijing Institute of Technology, Beijing 102488, PR China

ARTICLE INFO

Keywords:
Polyoxometalates
Ni-substitution
Water-soluble CdSe quantum dots
Photocatalytic hydrogen production

ABSTRACT

The development of robust and efficient hydrogen-evolving system remains a substantial but promising challenge to convert solar energy into clean fuel. Herein, we report the construction of water-compatible, robust, and ultraefficient hydrogen-evolving system by coupling water-soluble CdSe light-absorbers with Ni-substituted polyoxometalate (Ni-POM) catalysts and AA electron donor. Such facile catalytic system exhibits superior and robust hydrogen production activity to date even among known semiconductor/POM hybrids-based hydrogen production systems. Multiple stability experiments confirm the molecular stability of Ni-POM catalysts under turnover conditions. Various experimental and spectroscopic analyses reveal that the synergistic cooperation between high photostability of CdSe light-absorber, outstanding reversible multi-electron-transferring property of Ni-POM catalyst, and the fast hole-removing ability of AA electron donor account for the exceptional performance of present catalytic system. Our present work provides new research insights into the continued development of effective hydrogen-evolving systems through coupling other QDs-based light-absorbers and earth-abundant transition-metal-substituted POM catalysts.

1. Introduction

Concerning the rapid consumption of traditional fossil fuels and the emergence of consequent environmental problems, it is urgent for mankind to explore low-cost, sustainable, and environmentally friendly energy sources. Current research efforts focus on developing efficient, robust, inexpensive, and environmentally-benign catalytic water splitting systems. Hydrogen production from artificial photosynthesis (AP) is an intriguing approach to storing and converting solar energy into clean and renewable fuels [1–6]. Since early reports on molecular water-reducing systems in the late 1970s, researchers have devoted great efforts on developing the photocatalytic, which comprises $[Ru(bpy)_3]^{2+}$ and/or its derivatives as light absorbers with a suitable catalyst such as Pt, an electron mediator, and an electron sacrificial agent [7, 8]. Since then, extensive efforts have been devoted to developing precious-metal-free water reduction systems (WRCs) with more active and durable constituents made solely of earth-abundant elements. To date, although the experimental investigations and mechanistic studies of these systems have also achieved important progress [9–16], the challenge still remains in terms of developing cost-effective, robust, and efficient transition-metal-containing catalysts as well as photostable light-absorbers to realize hydrogen production from water under visible light irradiation.

In recent years, important progress has been made with respect to the development of photostable light-absorbers by using water-soluble semiconductor quantum dots (QDs) to drive proton reduction systems [17–33]. Compared with precious-metal-based organometallic chromophores (e.g. $Ru(bpy)_3^{2+}$) and the highly-luminescent organic dyes (e.g. Fluorescein and Eosin Y), semiconductor QDs exhibit important advantages of superior photostability, tunable redox potentials, size-dependent absorption properties, and large absorption cross sections across the visible spectrum, etc [34–38]. Some representative examples of using CdSe QDs as light-absorbers in visible-light-driven hydrogen evolution systems include: Eisenberg and co-workers reported aqueous proton reduction system containing dihydrolipoic acid (DHLA)-capped CdSe light absorber and a soluble Ni^{2+}-DHLA catalyst, which catalyzed hydrogen production with quantum yields of over 36% in 360 h under illumination at 520 nm [37]. Wu and co-workers

* Corresponding authors.
E-mail addresses: hlv@bit.edu.cn (H. Lv), ygy@bit.edu.cn (G.-Y. Yang).

https://doi.org/10.1016/j.apcatb.2021.120893
Received 17 September 2021; Received in revised form 27 October 2021; Accepted 1 November 2021
Available online 6 November 2021

reported a hydrogen production system using partially ZnS-covered CdSe QDs, achieving a constant hydrogen evolution rate of around 306.3 ± 21.1 μmol mg^{-1} h^{-1} during 40 h [39]. Despite of these impressive progress, most of these systems reported a photocatalytic hydrogen production rate below 10 mmol h^{-1} g^{-1}, which has strongly encouraged us to design more effective water reduction system by coupling QDs-based light-absorbers with more robust and efficient hydrogen-evolving catalysts. As an interesting type of multi-electron-transfer catalysts, earth-abundant transition-metal-substituted polyoxometalates (POMs) have attracted increasing attention in catalyzing hydrogen production in recent years due to their rich redox chemistry, electronic structure and compositional tunability, and excellent electron reservoir capacity, etc [20,40–53]. So far, there are very few reports on the integration of CdS nanomaterials with POMs for photocatalytic studies [54–58]; however, all of them are focused on the construction of heterogeneous nanocomposites in the presence of noble metal cocatalysts or other semiconductive supports (e.g. g-C_3N_4, carbon dots, graphene), which exhibited low catalytic efficiency in terms of turnover number (TON) or turnover frequency (TOF) comparing to that of homogeneous catalytic systems.

In this context, we report herein a water-compatible, robust, and ultraefficient hydrogen-evolving system by coupling water-soluble CdSe QDs light-absorbers with nickel-substituted polyoxometalate catalysts and AA electron donor. Upon green LED light irradiation, the resulting CdSe+POM catalytic system exhibits superior hydrogen production activity with a TON of 9000 versus tetra-Ni-substituted POM catalyst in 12-hour photocatalysis, corresponding to a hydrogen production rate of as high as 138 mmol g^{-1} h^{-1}, which is, to our knowledge, the highest value achieved to date even among known semiconductor/POM hybrids-based hydrogen production systems. Various experimental and spectroscopic analyses reveal that the exceptional performance of present catalytic system could be attributed to the synergistic cooperation between high photostability of CdSe light-absorber, outstanding reversible multi-electron-transferring property of Ni-substituted POM catalyst, and the fast hole-removing ability of AA electron donor.

2. Experimental

2.1. Materials and instrumentation

All starting chemicals and solvents for syntheses, characterization, and catalytic studies were purchased from commercial sources and were used as received without further purification unless otherwise noted. The deionized water was used for the photocatalytic H_2 evolution experiments. 3-Mercaptopropionic acid (MPA) were purchased from Damas and used as received. The trin-octylphosphine oxide-capped CdSe (CdSe-TOPO) QDs were prepared using slightly modified procedures to that reported previously [37]. The FT-IR spectra were measured on a Thermo Nicolet iS10 spectrometer. UV-Vis spectra were recorded on Techcomp UV 2600 spectrophotometer. UV-Vis spectra of CdSe-TOPO QDs were measured in hexane while those of water-soluble CdSe-MPA QDs were obtained in water. The steady-state photoluminescence spectra were recorded on a F97 Pro spectrofluorimeter and the fluorescence lifetime was recorded on a Edinburgh Instruments Life Spec II. Inductively coupled plasma mass spectrometry was performed by X Series 2 ICP-MS. X-ray photoelectron spectroscopy (XPS) data was carried out using PHI 5000 VersaProbe III Scanning XPS Microprobe. The capillary electrophoretic experiments were performed in a capillary electrophoretic apparatus UC 7010 equipped with Fused-silica capillaries (50 μm i.d., effective length 35 cm) at 200 nm detection wavelength; in a typical capillary electrophoretic test, 20 μM Ni-substituted POM catalyst solution was analyzed using either 20 mM sodium acetate buffer solution (pH 5.0 and 8.3) or 20 mM Borax (pH 10.0) as eluent. Thermogravimetric data were collected on Shimadzu DTG-60 & DSC-60instruments. Chopped-light chronoamperometric measurements were performed by CHI 660E using indium tin oxide (ITO) working electrode, Ag/AgCl (3 M KCl) reference electrode, and Pt wire auxiliary electrode. The surface morphology and chemical composition of film samples were determined by field emission scanning electron microscopy (JSM-7500 F) with a built-in EDS system. Transmission electron microscopy (TEM) images were taken on a JEM-2100 field emission microscope at an accelerating voltage of 200 kV. Analysis of hydrogen in the reaction headspace was performed using a Thermo GC7900 model gas chromatograph equipped with thermal conductivity detector (TCD) and a 5 Å molecular sieve capillary column.

2.2. Preparation

2.2.1. Synthesis of TOPO- or MPA-capped CdSe QDs

CdSe QDs were synthesized according to the modified literature method [37]. Briefly, 4.4 g of trioctylphosphine oxide (TOPO, 99%), 2.6 g of 1-hexadecylamine (HAD, ≥99%) and 0.08 g of n-tetradecylphosphonic acid (TDPA, 98%) were added into a 25 mL three-neck flask. The mixture was degassed under vacuum for 10 min and heated at 100 °C. Under Ar atmosphere, 1 mL of 1 M TOP-Se (prepared previously by dissolving 0.7894 g elemental Se shot in 10 mL TOP), was injected into the flask. Then, the solution was degassed under vacuum for another 10 min, switched to an N_2 atmosphere, and heated to 300 ºC. Meanwhile, 1.5 mL Cd-TOP (prepared by dissolving 0.72 g ($(CH_3COO)_2Cd{\cdot}3H_2O$ in 15 mL TOP) was injected swiftly. The temperature of solution was immediately changed to 260 ºC for CdSe nanocrystal growth, followed by cooling to room temperature. The final size of the CdSe nanocrystals was controlled by varying the growth time over several minutes. The water-soluble MPA-capped CdSe nanocrystals (CdSe-MPA) were synthesized through ligand exchange reactions in methanol under N_2 atmosphere [21,37,59]. Typically, the purified CdSe-TOPO QDs (0.05 mol) in hexane (1 mL) was mixed with 1 mL MPA-containing methanol solution (prepared by dissolving 0.106 g MPA and 0.067 g KOH in 20 mL methanol). The mixture was vigorously stirred until the CdSe QDs layer transferring to the methanol layer, which was finally precipitated out by adding 2 mL ether. The water-soluble CdSe-MPA QDs were dispersed into deionized water and stored in dark for further use.

2.2.2. Synthesis of $K_6Na[Ni_3(H_2O)_3PW_{10}O_{39}H_2O]{\cdot}12H_2O$ (K_6Na-Ni_3P)

The compound K_6Na-Ni_3P was synthesized following the procedures below [60]. Typically, a solution of 2.49 g (10 mmol) of Ni $(OOCCH_3)_2.4H_2O$ in 50 mL of water was added to 100 mL of an aqueous solution containing 9.87 g (33 mmol) of $Na_2WO_4.2H_2O$ and 0.425 g (3 mmol) of Na_2HPO_4 with pH adjusted to 6.5 with acetic acid. The resulting yellow solution (pH = 6.3) was refluxed for 2 h and hot filtered, and then 4 g of $K(OOCCH_3)$ was added to the filtrate while hot. After several days small pale green needle-shaped crystals of the desired product were isolated by filtration and dried under vacuum.

2.2.3. Synthesis of $Na_6K_4[Ni_4(H_2O)_2(PW_9O_{34})_2]{\cdot}24\ H_2O$ (Na_6K_4-Ni_4P_2)

The compound Na_6K_4-Ni_4P_2 was synthesized according to the modified literature method as follows [20]: $Na_2WO_4.2\ H_2O$ (33 g, 100 mmol) and Na_2HPO_4 (1.57 g, 11 mmol) were dissolved in 100 mL aqueous solution with the pH adjusted to 7.0 using concentrated acetic acid. To this was added slowly with vigorously stirring a solution of Ni $(OOCCH_3)_2.4\ H_2O$ (5.5 g, 22 mmol) in 50 mL aqueous solution. The resulting mixture was refluxed for 2.5 h and filtered hot to remove any precipitate, then 4 g of $K(OOCCH_3)$ was added and the hot yellow solution left for crystallization. Yellow crystals were isolated from the filtrate after several days and dried under vacuum.

2.2.4. Synthesis of $K_5Na_{11}[Ni_9(OH)_3(H_2O)_6(HPO_4)_2(PW_9O_{34})_3]{\cdot}55H_2O$ (K_5Na_{11}-Ni_9P_3)

The compound K_5Na_{11}-Ni_9P_3 was synthesized according to reported literature method as follows [60]: $Na_2WO_4.2\ H_2O$ (16.5 g, 50 mmol) and Na_2HPO_4 (0.78 g, 5.5 mmol) were dissolved in aqueous solution with the pH adjusted to 7.9 using acetic acid. To this was added a solution

containing $Ni(OOCCH_3)_2.4H_2O$ (4.1 g, 16 mmol) in 30 mL aqueous solution. The resulting green solution (pH = 7.5) was refluxed for 2 h. A 4 g amount of Na_2HPO_4 was added, and the solution was refluxed again for 9 h and hot filtered. After adding 5 g of solid $K(OOCCH_3)$, the resulting solution was allowed to cool at room temperature. After several hours small green needle-shaped crystals of the desired product were isolated by filtration and dried under vacuum.

2.2.5. Synthesis of $Na_{18}K_{10}[\{Ni_4(OH)_3PO_4\}_4(A\text{-}\alpha\text{-}PW_9O_{34})_4]\cdot 75H_2O$ ($Na_{18}K_{10}$-$Ni_{16}P_4$)

The compound $Na_{18}K_{10}$-$Ni_{16}P_4$ was synthesized according to the modified literature method as follows [61]: $Na_2WO_4.2H_2O$ (16.5 g, 50 mmol) and Na_2HPO_4 (0.78 g, 5.5 mmol) were dissolved in 80 mL aqueous solution and the pH adjusted to 8.10 by addition of concentrated acetic acid. To this solution was added slowly with vigorous stirring a solution of $Ni(OOCCH_3)_2.4H_2O$ (4.1 g, 16 mmol) in 35 mL aqueous solution. The resulting green solution was heated at reflux for 2 h. Then, a Na_2HPO_4 (4 g) was added and the resulting mixture was heated at reflux for another 9 h and filtered hot to remove any precipitate. The hot green solution was allowed to cool to room temperature and left for crystallization. Green needle-shaped crystals of the desired products were collected by filtration and dried under ambient conditions. For all four Ni-substituted POMs, their tetrabutylammonium salts (TBA-Ni_3P, TBA-Ni_4P_2, TBA-Ni_9P_3, and TBA-$Ni_{16}P_4$) were obtained using a cation-exchange approach [20,53].

2.3. The photocatalytic H_2 evolution tests

The light-driven hydrogen evolution experiments were performed in a cylindrical reaction flask with a total volume of ~10 mL. In a typical experiment, the cell was filled with 6.0 mL H_2O solution containing 2 μM CdSe-MPA QDs, 0.2 M ascorbic acid (AA), and 2 μM Ni-substituted POM catalyst at pH 4.5. The reaction cell was sealed with a rubber septum, carefully degassed and filled with Ar/CH_4 (4/1, volume ratio). All procedures were performed with a minimum exposure to ambient light. The reactor was illuminated under 520 nm green LED light with light intensity of 45 mW cm^{-2} of PCX50C instrument, Beijing PerfectLight Technology Co., Ltd. The post-reaction QDs could be isolated by centrifugation and further used for stability and recyclability tests.

Control experiments were carried out in the absence of each component (e.g. CdSe-MPA QDs, AA, or POM catalyst) under similar conditions as described above. More control experiments were performed by replacing catalyst Ni_4P_2 with either plenary Dawson-type $K_6[\alpha\text{-}P_2W_{18}O_{62}]$ (P_2W_{18}), tri-lacunary $Na_9[PW_9O_{34}]$ (PW_9), or $NiCl_2$ under otherwise identical conditions.

3. Results and discussion

3.1. Syntheses and characterization

Four nickel-substituted polyoxometalate (Ni_3P, Ni_4P_2, Ni_9P_3, and $Ni_{16}P_4$) complexes were prepared as described in above experimental section, their solid-state molecular structures were characterized by single-crystal X-ray diffraction that are consistent with the literature reports [20,60,61]. The polyhedral and ball-and-stick representations of these four polyoxoanions are shown in Fig. S1. The thermogravimetric (TGA) analyses confirmed the number of crystallized water molecules per formula unit of each polyoxometalate complex (Fig. S2). The FT-IR spectra of all four Ni-substituted POMs in 2 wt% KBr pellets exhibit the characteristic bands of POM structure in the range of 1200–400 cm^{-1}, the exchange of cation from Na^+/K^+ ions to tetrabutylammonium (TBA^+) does not change their FT-IR spectra (Fig. S3). The resulting TBA salt of Ni-substituted POMs were used as efficient molecular catalysts for hydrogen production in a three-component system upon visible light irradiation.

3.2. Characterization of CdSe QDs

The hydrophobic TOPO-capped CdSe QDs with different sizes were synthesized by hot-injection method as described in above Experimental section. The resulting CdSe QDs show controllable size-dependent UV-Vis absorption and photoluminescence (PL) spectra as shown in Figs. 1a and b. For simplicity, the obtained CdSe QDs were denoted as CdSe(540) for instance, herein the number 540 represents the absorption wavelength maximum of the first excitonic state. The representative TEM images (Fig. 1c) of the TOPO-capped CdSe(540) reveal nearly monodispersed spherical quantum dots with a mean size of 3.4 nm. The water-soluble MPA-capped CdSe QDs used for the photocatalytic experiments were prepared through ligand exchange of CdSe-TOPO QDs with the corresponding water-solubilizing capping agent MPA, of which the thiolates coordinate to surface Cd^{2+} and carboxylic acid groups significantly deprotonated at pH 4.5. TEM images of the CdSe-MPA QDs clearly indicate that the ligand exchange does not affect the size of CdSe QDs (Fig. S4), also their UV-Vis spectra of CdSe QDs before and after ligand exchange remain largely unchanged (Fig. S5).

3.3. Photocatalytic H_2 evolution activity

The MPA-capped water-soluble CdSe QDs were employed as light-absorbers in the photocatalytic H_2 evolution system owing to their superior photostability, larger absorption cross-sections over a broad spectral range, tunable electronic and optical properties, and the capacity to deliver multiple electrons with minimal structural perturbations. When coupling with Ni-substituted POM, Ni_4P_2, as the hydrogen-evolving catalyst and AA as the sacrificial electron donor, the three-component photocatalytic systems have achieved basically linear production of hydrogen with time in deaerated aqueous solution upon 520 nm green LED light irradiation (Fig. 2). Previous studies have shown that the net stored energy in the presence of AA as the sacrificial electron donor reaches approximately 20 kcal/mol while being oxidized to dehydroascorbic acid (AA^+), indicating that such three-component photocatalytic system is indeed an energy-storing process [7,59,62]. Herein, the AA could serve as both a potential source of hydrogen and as a buffer with its conjugate base (AA^+), helping to maintain the acidic pH even as protons are reduced to hydrogen. The influences of pH on the hydrogen production are shown in Fig. S6. The hydrogen evolution rate and yield gradually increased with the raising pH value, reaching an optimal value of pH = 4.5. Such experimental results are understandable because lower pH value than 4.5 will lead to declining electron-donating ability of AA, while higher pH value is thermodynamically unfavorable for proton reduction to hydrogen. Considering the size-dependent electronic properties of CdSe QDs, the reduction potential of the excited states of CdSe QDs could be readily controlled by the nanocrystal size. We firstly investigated the hydrogen production performance using different-sized CdSe-MPA QDs. As expected, the generation rate of H_2 is closely related to the size of QDs (Fig. 2), the photocatalytic H_2 production activity increases with the decreasing size from CdSe(580) to CdSe(540), which could be attributed to the increase of reducing power of smaller-sized CdSe(540). However, further decreasing the QDs size from CdSe(540) to CdSe(510) leads to slightly lower hydrogen production rate, which could be ascribed to less amount of captured photons given the fact that the QDs absorption edge is to the blue of the light-emitting diode (LED) spectral emission profile. Therefore, the MPA-capped CdSe(540) QDs were used for the following photocatalytic experiments.

To better understand the photocatalytic process, we have systematically optimized the photocatalytic reaction system. Photolysis of the reaction solution containing 2 μM CdSe-MPA(540), 2 μM Ni_4P_2, and 0.2 M AA results in efficient generation of hydrogen under green LED light irradiation. It is noted that the catalytic turnover number (TON) was calculated by dividing the moles of photogenerated hydrogen to the moles of Ni_4P_2 catalyst. After 12 h reaction, around 108 μmol hydrogen

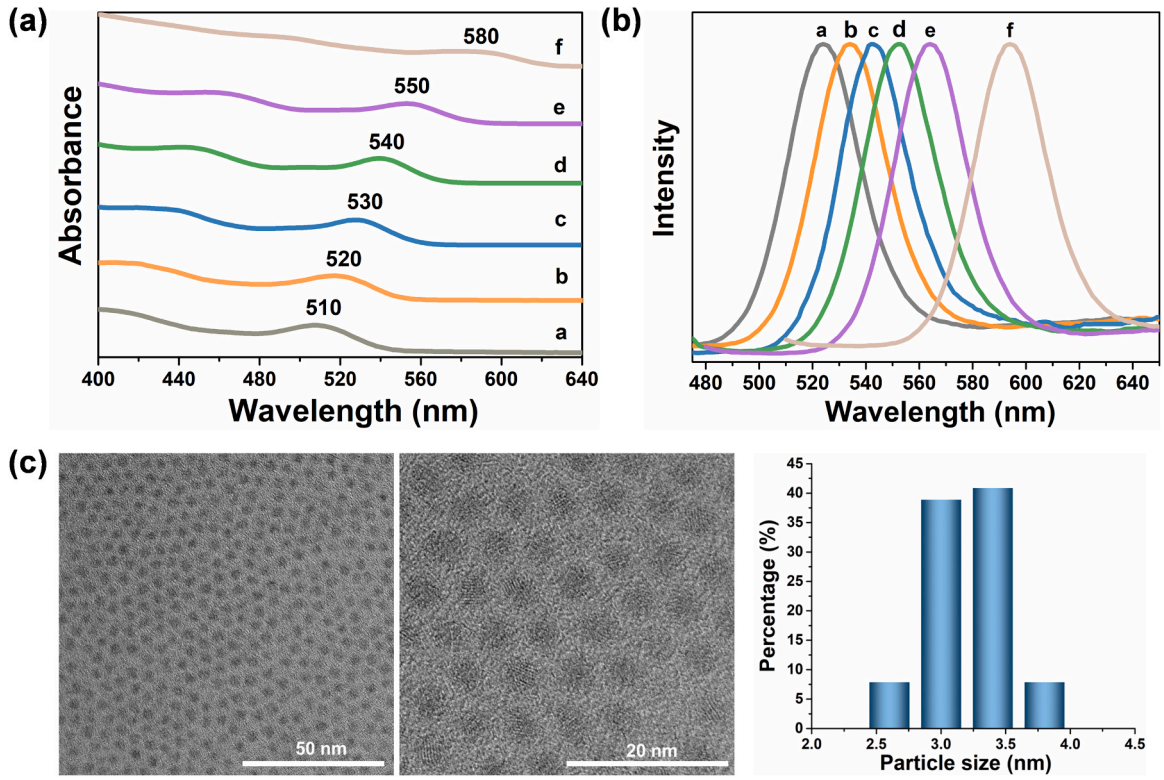

Fig. 1. (a) UV-Vis absorption; (b) Photoluminescence spectra for CdSe-TOPO QDs in hexane and (c) Bright field TEM images (scale bars: 50 nm and 20 nm, respectively) and corresponding size distribution of CdSe-TOPO(540), the average diameter was calculated to be 3.4 ± 0.41 nm by counting 100 particles.

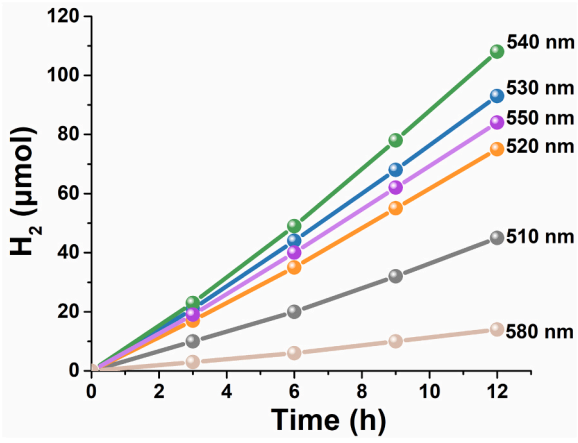

Fig. 2. H_2 production from irradiation of aqueous solutions using 2 μM CdSe-MPA QDs with different sizes labeled by the peak in their first excitonic absorption, 2 μM Ni_4P_2, and 0.2 M AA in 6 mL H_2O at pH = 4.5 upon irradiation with 520 nm LED at 15 °C and 1 atm initial pressure of Ar/CH_4 (4/1, volume ratio) with CH_4 as an internal standard for H_2 quantification by GC analysis.

was produced, corresponding to a TON of 9000 (Fig. 3a). The calculated hydrogen production rate versus the mass of Ni_4P_2 catalyst reached as high as 138 mmol g^{-1} h^{-1}, which is, to our knowledge, the highest value achieved to date even among those semiconductor/POM hybrids-based hydrogen production systems [57,58,63]. The detailed comparison was summarized in Table S1. Control experiments in the absence of each component (CdSe-MPA QDs, AA, or Ni_4P_2) leads to negligible generation of hydrogen (Fig. 3a). Further control experiments using either plenary Dawson-type P_2W_{18} or trilacunary PW_9 in place of Ni_4P_2 catalyst yields very small amount of hydrogen production, indicating that transition metal Ni could work as the active sites for efficient photocatalysis (Fig. 3a). In addition, another important control experiment using equivalent moles of $NiCl_2$ (8 μM) under otherwise identical conditions also produces much less amount of hydrogen (30 μmol, Fig. 3a, orange line). Above experimental results revealed that the specific molecular structure of Ni_4P_2 catalyst is crucial for ultraefficient photocatalytic generation of hydrogen. The empty 5d orbitals in the W centers of the trilacunary PW_9 ligand exhibit outstanding reversible multi-electron-storing property, thereby working as the electron-storage sponge to facilitate the effective separation of the photogenerated charge carriers in CdSe-MPA QDs, which are consistent with literature observations in those semiconductor/POM nanohybrids [51,54,56,64]. The rates and yields of hydrogen production also depend on the concentrations of Ni_4P_2 catalyst, CdSe-MPA QDs, and the AA electron donor, respectively. Varying the concentration of Ni_4P_2 catalyst from 1 to 4 μM leads to a steady increase of hydrogen yield from 69 to 128 μmol after 12-hour photocatalysis (Fig. 3b). In addition, an increase of CdSe-MPA QDs concentration from 1 to 4 μM results in growth of hydrogen production from 46 to 150 μmol, corresponding to an enhancement of TON from 3830 to 12500 (Fig. S7). Whereas the concentration of AA electron also shows positive effect on hydrogen generation; however, the saturation could be approached at concentrations greater than 0.4 M (Fig. S8), revealing that the hole-removing process from the photoexcited CdSe-MPA QDs is no longer the rate-limiting step at very high concentration of AA. More importantly, the critical role of CdSe-MPA light-absorbers was further confirmed by delicately-designed experiments using the commercially-available organometallic chromophores ($[Ir(ppy)_2(dtbbpy)]^+$ and $[Ru(bpy)_3]^{2+}$) to replace CdSe-MPA QDs. At the same concentration of photosensitizer and Ni_4P_2 catalyst, the CdSe-MPA-containing catalytic system achieved 3000-fold and 300-fold higher TONs than that of $[Ir(ppy)_2(dtbbpy)]^+$-containing and $[Ru(bpy)_3]^{2+}$-containing systems, respectively (Fig. S9a, Table S2). In addition, the TONs obtained in those organometallic chromophore-containing systems are still much lower even at much higher concentrations of Ni_4P_2 catalyst and the chromophores (Fig. S9b,

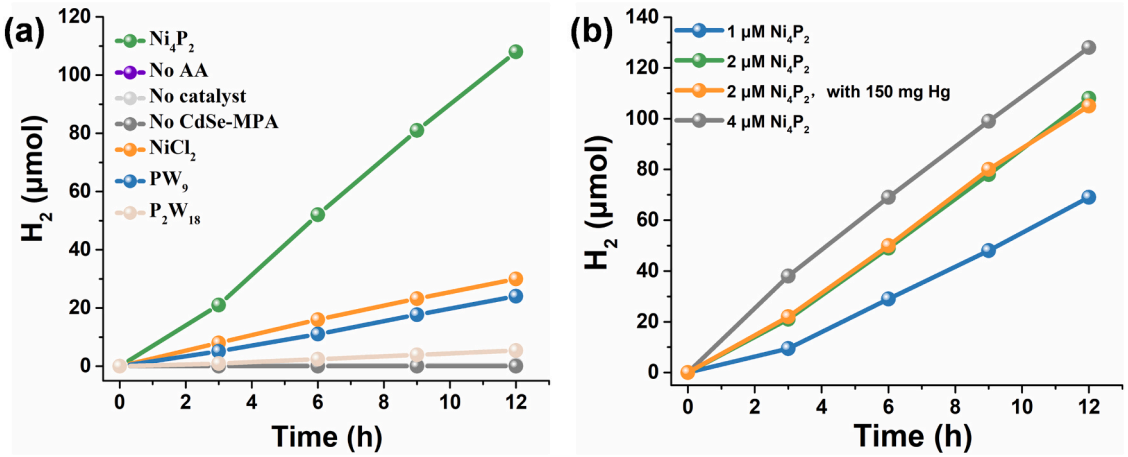

Fig. 3. Photocatalytic H_2 evolution as a function of (a) different catalysts; and (b) different concentrations of catalyst 1–4 μM **Ni_4P_2** and mercury-poison test. Standard conditions: 2 μM CdSe-MPA QDs(540), 0.2 M AA, 2 μM **Ni_4P_2**, 6 mL H_2O at pH = 4.5 upon irradiation with 520 nm LED at 15 °C and 1 atm initial pressure of Ar/CH_4 (4/1) with CH_4 as an internal standard for H_2 quantification by GC analysis.

Table S2). These results strongly confirmed that the superior light-absorbing ability, high photostability, together with the synergistically effective coupling with the multi-electron-transfer Ni_4P_2 catalyst are indispensable for efficient visible-light-driven generation of hydrogen. Also, it is worth mentioning that our present photocatalytic system could be readily applicable for other multi-nuclearity Ni-substituted POMs (e.g. Ni_3P, Ni_9P_3, and $Ni_{16}P_4$). Photocatalytic hydrogen production experiments show that all three Ni-substituted POM catalysts can efficiently catalyze the generation of hydrogen under the otherwise identical conditions, the hydrogen yields and TONs are positively associated with the nuclearity of Ni centers in a given reaction time (Table S3). which should be attributed to the increase in catalytic active sites of the multinuclear transition metal substituted POM-based molecular catalysts (Table S3). Such experimental evidence elucidates the possibility of exploring other types of multi-nuclearity transition-metal-substituted POM catalyst using our facile CdSe+POM photocatalytic system.

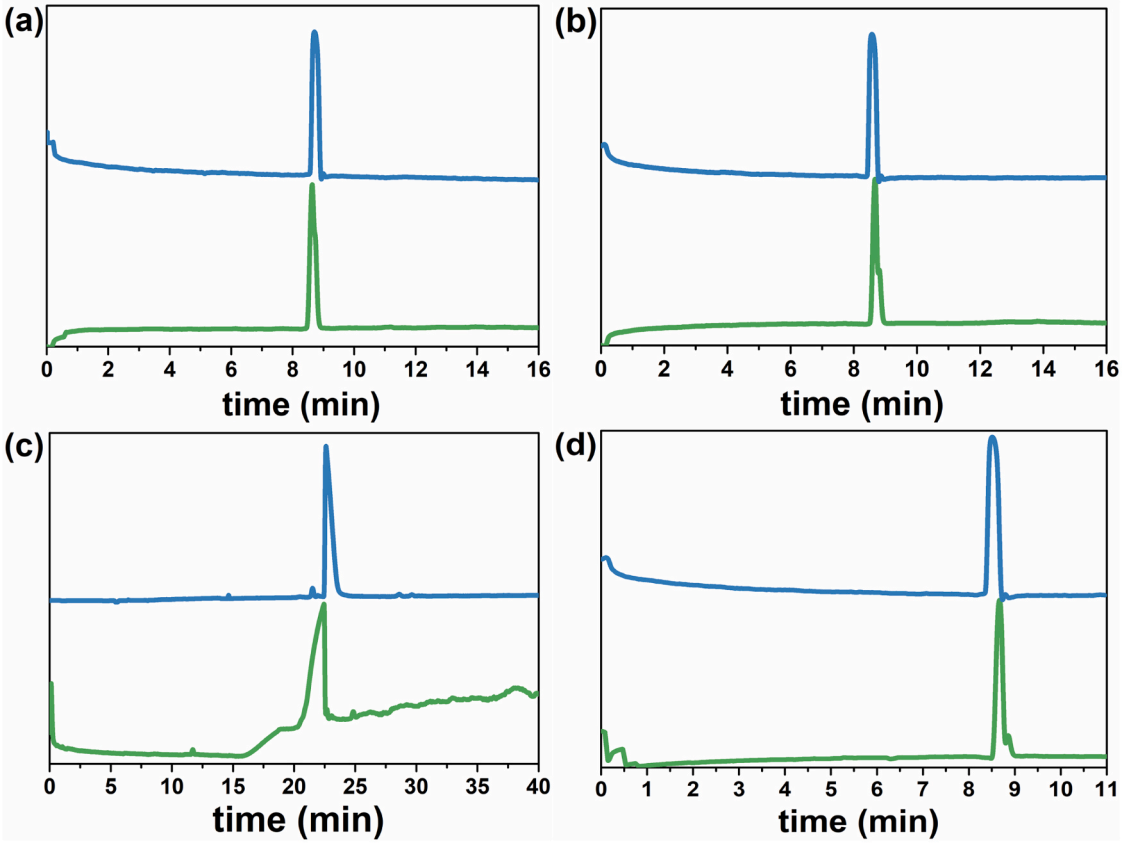

Fig. 4. Capillary electrophoresis measurements on (a) Ni_3P, (b) Ni_4P_2, (c) Ni_9P_3, (d) $Ni_{16}P_4$ before (blue curve) and after (green curve) photocatalytic reactions at catalyst concentration of 20 μM.

3.4. Stability and robustness evaluation

As a molecular multi-electron-transfer hydrogen-evolving catalyst, the stability of Ni_4P_2 catalyst under turnover conditions has been investigated using multiple physicochemical approaches. First, a mercury-poison test (using up to 150 mg Hg) has been carried out to exclude the possible formation of metal nanoparticles from the decomposition of Ni_4P_2 catalyst under turnover conditions. Almost identical hydrogen production rate and yield were obtained in such mercury-poisoning experiment as that of the catalytic system in the absence of Hg (Fig. 3b, orange and green lines), proving the integrity of Ni_4P_2 catalyst under turnover conditions. Also, it is noted that the hydrogen yield from mercury-poison test is much higher than that of using molar equivalents of $NiCl_2$ (8 μM) as catalyst, further revealing that its intact molecular structure of Ni_4P_2 catalyst is vital for efficient catalysis. Second, the ICP analyses on the post-reaction solution revealed that the content of Ni and W elements remained basically unchanged before and after photocatalysis (Table S4), further supporting the molecular nature of Ni_4P_2 catalyst during hydrogen evolution process. Third, the capillary electrophoresis measurements before and after photocatalysis exhibit same retention time of the Ni_4P_2 catalyst signals (Fig. 4), supporting the conclusion that Ni_4P_2 catalyst retain its molecular integrity during photocatalysis. Similar experimental results were also observed while using other three Ni-substituted POM catalysts (Ni_3P, Ni_9P_3, and $Ni_{16}P_4$; Fig. 4).

In addition to above experimental evidence, we have also carefully compared and characterized the CdSe QDs isolated from the post-reaction solution using $NiCl_2$ or Ni_4P_2 as catalyst. EDS analyses and SEM/elemental mapping on the post-isolated CdSe QDs from the $NiCl_2$-catalytic system clearly show the presence of Ni signal (Fig. S10), indicating the deposition of Ni element on the surface of CdSe QDs. Also, addition of freshly-prepared CdSe-MPA QDs into the centrifuged post-reaction solution of $NiCl_2$-catalyzed system cannot recover its catalytic activity, proving the heterogeneity of the $NiCl_2$-catalytic system under turnover conditions. Such phenomenon does not exist in the Ni_4P_2-based catalytic system. Moreover, no signal of Ni element was observed on the post-isolated CdSe QDs from the Ni_4P_2-catalyzed system according to the EDS analyses (Fig. S11) and SEM/elemental mapping results (Fig. 5a). Considering the relative low sensitivity of EDS mapping technique, XPS technique was further utilized to characterize the surface composition of the post-isolated CdSe QDs. XPS spectrum shows the presence of Cd, Se, and S signals in CdSe-MPA QDs, but no Ni signal was observed (Fig. S12, Fig. 5b), which is consistent with above experimental results. In addition, we have also compared the FT-IR spectra of Ni_4P_2 catalyst before and after 12-hour photocatalysis. As shown in Fig. S13, the FT-IR spectra remained basically unchanged before and after photocatalysis, further confirming the molecular integrity of Ni_4P_2 catalyst. All these observations fully confirmed that the Ni_4P_2 catalyst basically remains its molecular nature under present photocatalytic hydrogen evolution conditions.

The long-term robustness and reusability of system components were further assessed by several additional experiments. To evaluate the robustness of the CdSe-MPA light-absorbers, post-reaction CdSe-MPA QDs were isolated from initial catalytic runs by centrifugation and then redispersed in slightly basic water for subsequent catalytic experiments. The UV-Vis spectra of solutions of isolated and freshly prepared CdSe-MPA QDs exhibit similar absorption profiles even after 12-hour photocatalysis (Fig. S14), proving their high photostability. Visible-light-driven hydrogen evolution experiments using isolated CdSe-MPA QDs plus fresh catalyst and AA solution in the second catalytic run produce similar hydrogen generation rates and yields to the results of the initial catalytic run using fresh CdSe-MPA QDs (Fig. 6a, green and orange lines), indicating the relatively high photostability of the CdSe-MPA light absorbers during the tested periods of photolysis. Further using the isolated CdSe-MPA QDs for the third-round photocatalysis leads to a slight decrease of H_2 yield, which might be caused by either the loss of QDs during centrifugation or MPA ligand dissociation after successive photocatalysis. In addition, a long-term catalytic experiment up to 6 days was conducted to better evaluate the long-term robustness of our present photocatalytic system. After 6 days photocatalysis, a TON of up to 33830 (corresponding to 406 μmol hydrogen) was achieved. It is noted that the hydrogen production rate slightly declines with the consumption of AA electron donor during long-term photocatalysis, but the activity restores when additional fresh AA solution was refilled into the catalytic system, further supporting the high stability of both CdSe-MPA light-absorbers and Ni_4P_2 catalyst.

3.5. Proposed photocatalytic mechanism

To elucidate the photocatalytic mechanism, we have conducted a series of characterizations on the integrated reaction system involving Ni_4P_2 catalyst, CdSe-MPA light-absorber, and AA electron donor. Excitation of the CdSe-MPA(540) ($\lambda_{excitation}$ = 450 nm) in HAc/NaAc buffer solution (pH=4.5) results in an obvious emission band in the

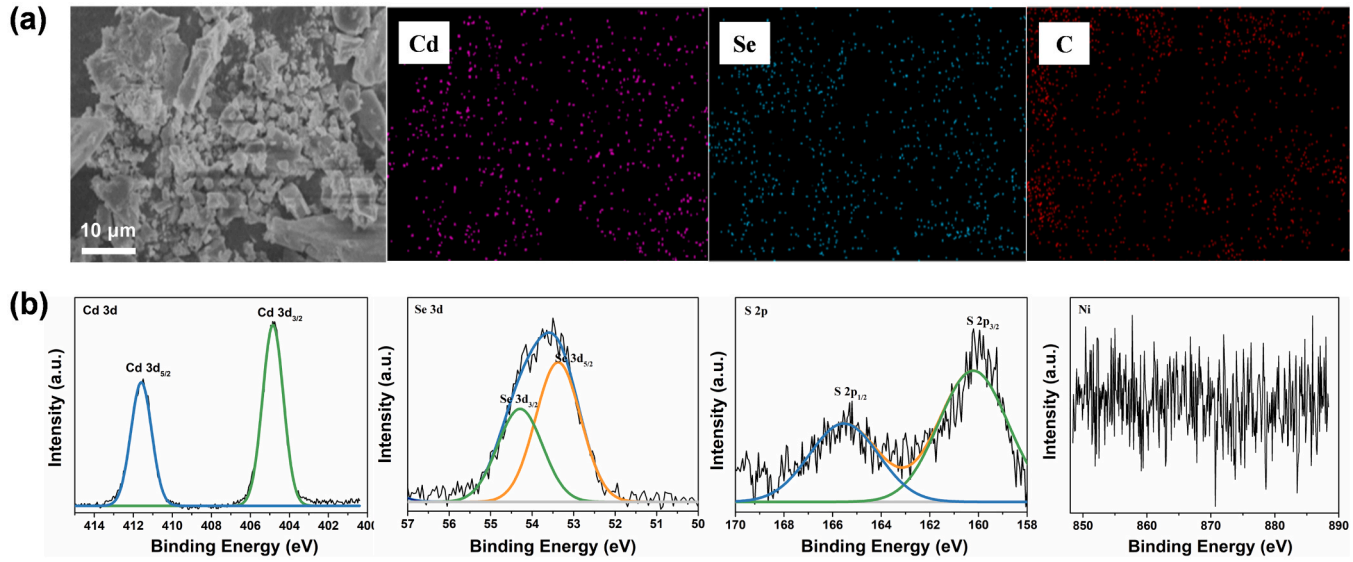

Fig. 5.. (a) SEM and corresponding elemental mapping images and (b) High resolution XPS spectra of Cd 3d, Se 3d, S 2p, and Ni 2p of isolated CdSe-MPA QDs after photocatalysis.

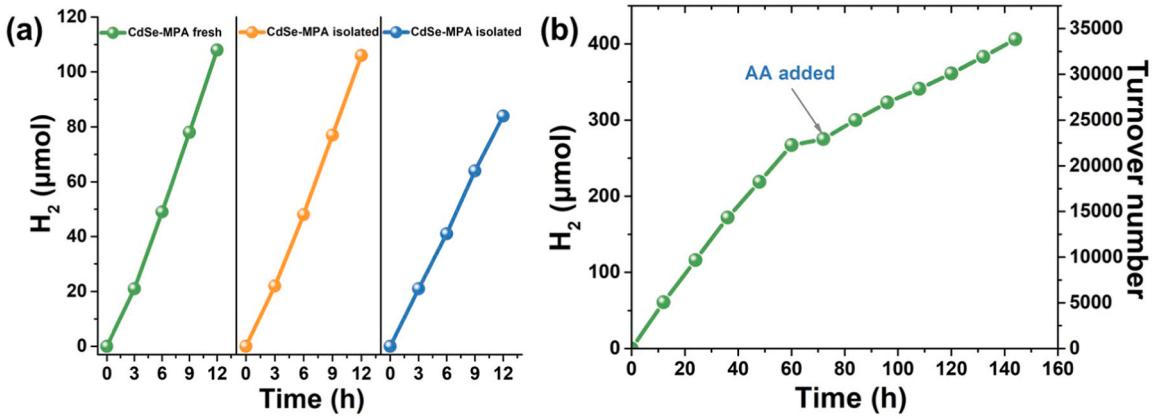

Fig. 6. (a) The photocatalytic recycling tests using fresh 2 μM CdSe-MPA(540) QDs (green curve) and isolated 2 μM CdSe-MPA(540) QDs (orange and blue curves); and (b) Long-term photocatalytic hydrogen production experiment over the system including 2 μM CdSe-MPA QDs(540), 2 μM Ni_4P_2, 0.2 M AA in 6.0 mL H_2O at pH 4.5 upon irradiation with 520 nm LED.

520–600 nm region. As shown in Fig. S15, the addition of both Ni_4P_2 catalyst and AA can lead to obvious emission quenching of the CdSe-MPA light-absorber, indicating that the photogenerated electrons and holes can both be efficiently quenched by Ni_4P_2 catalyst and AA electron donor, respectively. Such quenching process were further studied using time-resolved photoluminescence spectroscopy. Fig. 7 illustrates the single exponential decay kinetics of the CdSe-MPA excited state luminescence in the presence of Ni_4P_2 catalyst and AA, yielding lifetimes of approximately 14.17 and 5.83 ns, respectively, which were shorter than that of CdSe-MPA alone (19.43 ns). The steady-state emission quenching and time-resolved luminescence decay results proved that the excited state of CdSe-MPA light absorber can be both oxidatively quenched by the Ni_4P_2 catalyst and reductively quenched by AA electron donor, also the reductive quenching process is the dominant one considering the much shorter lifetime and the relatively higher concentration of AA. To better understand those quenching processes, the chopped-light chronoamperometric measurements were carried out to investigate the separation efficiency of the photogenerated electron-hole pairs (Fig. S16). While using an ITO as working electrode, the dispersed CdSe-MPA in HAc/NaAc buffer solution exhibits very weak cathodic photocurrent upon green LED light irradiation. Such cathodic photocurrent response was slightly enhanced in the presence of Ni_4P_2 catalyst, indicating the facilitated photogenerated electrons migration from CdSe-QDs to Ni_4P_2 catalyst in solution. In contrast, when AA was present in solution, a remarkable enhancement of anodic photocurrent was achieved upon light irradiation (Fig. S16). This experimental result implies the ultraefficient removal of photogenerated holes in CdSe-MPA QDs by AA electron donor, thereby pushing photogenerated electrons to the external circuit to produce anodic photocurrent. Overall, the presence of Ni_4P_2 catalyst and AA electron donor could, to a large extent, facilitate the separation and migration of photogenerated electron-hole pairs in photoexcited states of CdSe-MPA QDs under visible light, thereby boosting the photocatalytic hydrogen production activity.

Based on all above experimental analyses, we proposed herein the photocatalytic mechanism for this CdSe+POM coupling system for visible-light-driven hydrogen evolution (Scheme 1). Upon visible light irradiation, CdSe-MPA QDs was photoexcited to produce the photogenerated electron-hole pairs. The photogenerated holes located in the VB of CdSe-MPA QDs will be preferentially scavenged by sacrificial reagents AA in the reaction system. Meanwhile, the leftover photogenerated electrons located in CB of CdSe-MPA QDs would be transferred to the Ni_4P_2 catalyst, where the solution protons will be reduced to hydrogen, finally accomplishing a full catalytic cycle. During the proton reduction process, the terminal labile aqua ligands could dissociate from the two external Ni centers and generate vacant sites for the formation of Ni-H species that further interact with H^+ to produce hydrogen gas as illustrated in our previous works [52,65]. Overall, the synergistic cooperation between high photostability of CdSe light-absorber, outstanding reversible multi-electron-transferring property of Ni_4P_2 catalyst, and the fast hole-removing ability of AA electron donor contribute to the exceptional performance of our reported catalytic system.

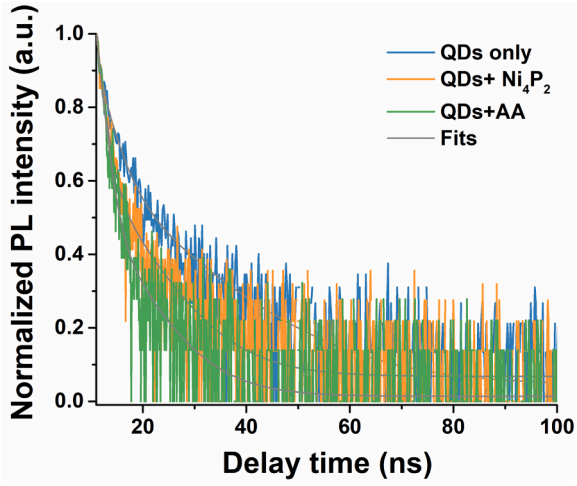

Fig. 7. Normalized luminescence decay kinetics of CdSe-MPA QDs (blue curve), CdSe-MPA QDs with Ni_4P_2 (orange curve), and CdSe-MPA QDs with AA (green curve). Conditions: 450 nm excitation, 2 μM CdSe-MPA QDs, 30 μM catalyst Ni_4P_2 and 0.2 M AA. The grey curves are best fits according to bi-exponential decay.

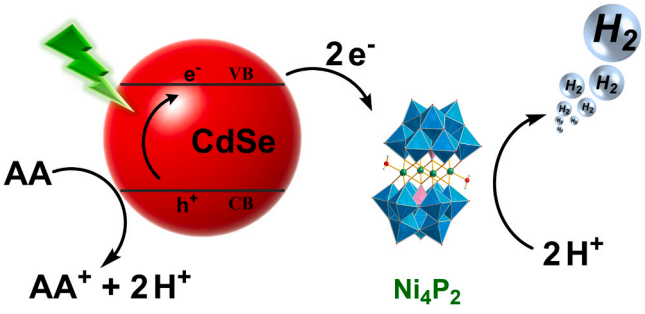

Scheme 1. Proposed mechanism of present catalytic system visible-light-driven H_2 evolution.

4. Conclusion

In summary, we have constructed a water-compatible, robust, and ultraefficient hydrogen-evolving system by coupling water-soluble CdSe QDs light-absorbers with nickel-substituted polyoxometalate catalysts and AA electron donor. Upon visible light irradiation, the present CdSe+POM catalytic system exhibits superior and robust hydrogen production activity to date even among known semiconductor/POM hybrids-based hydrogen production systems. Under minimally optimized conditions, the Ni_4P_2-catalyzed reaction system achieved a TON of up to 9000 after 12-hour photocatalysis, corresponding to the calculated hydrogen production rate of as high as 138 mmol g^{-1} h^{-1}, which is way much efficient than that of organometallic chromophore-containing catalytic systems. The present facile catalytic system is also applicable for other multi-nuclearity Ni-substituted POM catalysts, and the activity is positively associated with the nuclearity of Ni centers in POM catalysts. Multiple stability experiments (including mercury-poison test, ICP analyses, capillary electrophoresis measurements, SEM/EDS, and XPS characterization, etc.) confirm the molecular stability of Ni-substituted POM catalysts under catalytic turnover conditions. Various experimental and spectroscopic analyses reveal that the synergistic cooperation between high photostability of CdSe light-absorber, outstanding reversible multi-electron-transferring property of Ni-substituted POM catalyst, and the fast hole-removing ability of AA electron donor account for the exceptional performance of present catalytic system. Our present work provides new research insights into the continued development of effective hydrogen-evolving systems through coupling other QDs-based light-absorbers and earth-abundant transition-metal-substituted POM catalysts.

CRediT authorship contribution statement

Mo Zhang: Data curation, Formal analysis, Investigation, Writing - original draft preparation. **and Xing Xin**: Software, Visualization. **Yeqin Feng:** Validation. **Junhao Zhang**: Software. **Hongjin Lv:** Funding acquisition, Project administration, Conceptualization, Supervision, Validation, Writing - reviewing & editing. **Guo-Yu Yang:** Funding acquisition, Supervision.

Declaration of Competing Interest

The authors declare that they have no known competing financial interests or personal relationships that could have appeared to influence the work reported in this paper.

Acknowledgements

We gratefully acknowledge the financial support from the National Natural Science Foundation of China (21871025 and 21831001); the Recruitment Program of Global Experts (Young Talents) and BIT Excellent Young Scholars Research Fund; the instrumental support from the Analysis and Testing Center of Beijing Instituted of Technology is also highly appreciated.

Appendix A. Supporting information

Supplementary data associated with this article can be found in the online version at doi:10.1016/j.apcatb.2021.120893.

References

[1] M. Graetzel, Artificial photosynthesis: water cleavage into hydrogen and oxygen by visible light, Acc. Chem. Res. 14 (1981) 376–384.
[2] N.S. Lewis, D.G. Nocera, Powering the planet: chemical challenges in solar energy utilization, Proc. Natl. Acad. Sci. U. S. A. 103 (2006) 15729–15735.
[3] H.B. Gray, Powering the planet with solar fuel, Nat. Chem. 1 (2009) 7, 7.
[4] R. Eisenberg, Chemistry. Rethinking water splitting, Science 324 (2009) 44–45.
[5] H. Nishiyama, T. Yamada, M. Nakabayashi, Y. Maehara, M. Yamaguchi, Y. Kuromiya, H. Tokudome, S. Akiyama, T. Watanabe, R. Narushima, S. Okunaka, N. Shibata, T. Takata, T. Hisatomi, K. Domen, Photocatalytic solar hydrogen production from water on a 100 m^{2-} scale, Nature 598 (2021) 304–307.
[6] H.L. Wu, X.B. Li, C.H. Tung, L.Z. Wu, Recent advances in sensitized photocathodes: from molecular dyes to semiconducting quantum dots, Adv. Sci. 5 (2018) 1700684.
[7] G.M. Brown, B.S. Brunschwig, C. Creutz, J.F. Endicott, N. Sutin, Homogeneous catalysis of the photoreduction of water by visible light. Mediation by a tris(2,2′-bipyridine)ruthenium(II)-cobalt(II) macrocycle system, J. Am. Chem. Soc. 101 (1979) 1298–1300.
[8] P.J. DeLaive, B.P. Sullivan, T.J. Meyer, D.G. Whitten, Applications of light-induced electron-transfer reactions. Coupling of hydrogen generation with photoreduction of ruthenium(II) complexes by triethylamine, J. Am. Chem. Soc. 101 (1979) 4007–4008.
[9] Z. Han, R. Eisenberg, Fuel from water: the photochemical generation of hydrogen from water, Acc. Chem. Res. 47 (2014) 2537–2544.
[10] Z. Wang, C. Li, K. Domen, Recent developments in heterogeneous photocatalysts for solar-driven overall water splitting, Chem. Soc. Rev. 48 (2019) 2109–2125.
[11] A.J. Esswein, D.G. Nocera, Hydrogen production by molecular photocatalysis, Chem. Rev. 107 (2007) 4022–4047.
[12] J.P. McEvoy, G.W. Brudvig, Water-splitting chemistry of photosystem II, Chem. Rev. 106 (2006) 4455–4483.
[13] Y. Liu, Z. Zhang, Y. Fang, B. Liu, J. Huang, F. Miao, Y. Bao, B. Dong, IR-driven strong plasmonic-coupling on Ag nanorices/$W_{18}O_{49}$ nanowires heterostructures for photo/thermal synergistic enhancement of H_2 evolution from ammonia borane, Appl. Catal. B: Environ. 252 (2019) 164–173.
[14] D. Dong, C. Yan, J. Huang, N. Lu, P. Wu, J. Wang, Z. Zhang, An electron-donating strategy to guide the construction of MOF photocatalysts toward co-catalyst-free highly efficient photocatalytic H_2 evolution, J. Mater. Chem. A 7 (2019) 24180–24185.
[15] M. Zhang, H. Li, J. Zhang, H. Lv, G.-Y. Yang, Research advances of light-driven hydrogen evolution using polyoxometalate-based catalysts, Chin. J. Catal. 42 (2021) 855–871.
[16] X. Jing, N. Lu, J. Huang, P. Zhang, Z. Zhang, One-step hydrothermal synthesis of S-defect-controlled $ZnIn_2S_4$ microflowers with improved kinetics process of charge-carriers for photocatalytic H_2 evolution, J. Energy Chem. 58 (2021) 397–407.
[17] G. Wang, X. Yang, F. Qian, J.Z. Zhang, Y. Li, Double-sided CdS and CdSe quantum dot co-sensitized ZnO nanowire arrays for photoelectrochemical hydrogen generation, Nano Lett. 10 (2010) 1088–1092.
[18] H. Zhu, N. Song, H. Lv, C.L. Hill, T. Lian, Near unity quantum yield of light-driven redox mediator reduction and efficient H_2 generation using colloidal nanorod heterostructures, J. Am. Chem. Soc. 134 (2012) 11701–11708.
[19] L. Amirav, A.P. Alivisatos, Photocatalytic hydrogen production with tunable nanorod heterostructures, J. Phys. Chem. Lett. 1 (2010) 1051–1054.
[20] H. Lv, W. Guo, K. Wu, Z. Chen, J. Bacsa, D.G. Musaev, Y.V. Geletii, S.M. Lauinger, T. Lian, C.L. Hill, A noble-metal-free, tetra-nickel polyoxotungstate catalyst for efficient photocatalytic hydrogen evolution, J. Am. Chem. Soc. 136 (2014) 14015–14018.
[21] H. Lv, C. Wang, G. Li, R. Burke, T.D. Krauss, Y. Gao, R. Eisenberg, Semiconductor quantum dot-sensitized rainbow photocathode for effective photoelectrochemical hydrogen generation, Proc. Natl. Acad. Sci. U. S. A. 114 (2017) 11297–11302.
[22] J. Zhao, M.A. Holmes, F.E. Osterloh, Quantum confinement controls photocatalysis: a free energy analysis for photocatalytic proton reduction at CdSe nanocrystals, ACS Nano 7 (2013) 4316–4325.
[23] F. Ehrat, T. Simon, J.K. Stolarczyk, J. Feldmann, Size effects on photocatalytic H_2 generation with CdSe/CdS core-shell nanocrystals, Z. Phys. Chem. 229 (2015) 205–219.
[24] Z.-J. Li, X.-B. Fan, X.-B. Li, J.-X. Li, F. Zhan, Y. Tao, X. Zhang, Q.-Y. Kong, N.-J. Zhao, J.-P. Zhang, C. Ye, Y.-J. Gao, X.-Z. Wang, Q.-Y. Meng, K. Feng, B. Chen, C.-H. Tung, L.-Z. Wu, Direct synthesis of all-inorganic heterostructured CdSe/CdS QDs in aqueous solution for improved photocatalytic hydrogen generation, J. Mater. Chem. A 5 (2017) 10365–10373.
[25] R. Bera, A. Dutta, S. Kundu, V. Polshettiwar, A. Patra, Design of a CdS/CdSe heterostructure for efficient H_2 generation and photovoltaic applications, J. Phys. Chem. C. 122 (2018) 12158–12167.
[26] R. Burke, N.M.B. Cogan, A. Oi, T.D. Krauss, Recovery of active and efficient photocatalytic H_2 production for CdSe quantum Dots, J. Phys. Chem. C. 122 (2018) 14099–14106.
[27] J.-X. Jian, C. Ye, X.-Z. Wang, M. Wen, Z.-J. Li, X.-B. Li, B. Chen, C.-H. Tung, L.-Z. Wu, Comparison of H_2 photogeneration by [FeFe]-hydrogenase mimics with CdSe QDs and $Ru(bpy)_3Cl_2$ in aqueous solution, Energy Environ. Sci. 9 (2016) 2083–2089.
[28] P. Wang, M. Wang, J. Zhang, C. Li, X. Xu, Y. Jin, Shell thickness engineering significantly boosts the photocatalytic H_2 evolution efficiency of CdS/CdSe core/shell quantum dots, ACS Appl. Mater. Interfaces 9 (2017) 35712–35720.
[29] F. Qiu, Z. Han, J.J. Peterson, M.Y. Odoi, K.L. Sowers, T.D. Krauss, Photocatalytic hydrogen generation by CdSe/CdS nanoparticles, Nano Lett. 16 (2016) 5347–5352.
[30] Y.-J. Yuan, D.-Q. Chen, M. Xiong, J.-S. Zhong, Z.-Y. Wan, Y. Zhou, S. Liu, Z.-T. Yu, L.-X. Yang, Z.-G. Zou, Bandgap engineering of $(AgIn)_xZn_{2(1-x)}S_2$ quantum dot photosensitizers for photocatalytic H_2 generation, Appl. Catal. B: Environ. 204 (2017) 58–66.
[31] L.K. Putri, B.-J. Ng, W.-J. Ong, H.W. Lee, W.S. Chang, A.R. Mohamed, S.-P. Chai, Energy level tuning of CdSe colloidal quantum dots in ternary ^0D–^2D-2D CdSe QD/B-rGO/O-gC_3N_4 as photocatalysts for enhanced hydrogen generation, Angew. Chem. Int. Ed. 265 (2020) 118592–118605.

[32] S. Raheman Ar, H.M. Wilson, B.M. Momin, U.S. Annapure, N. Jha, CdSe quantum dots modified thiol functionalized g-C_3N_4: intimate interfacial charge transfer between 0D/2D nanostructure for visible light H_2 evolution, Renew. Energy 158 (2020) 431–443.
[33] X. Xiang, B. Zhu, B. Cheng, J. Yu, H. Lv, Enhanced photocatalytic H_2-production activity of CdS quantum dots using Sn^{2+} as cocatalyst under visible light irradiation, Small 16 (2020) 2001024–2001033.
[34] J. Jasieniak, M. Califano, S.E. Watkins, Size-dependent valence and conduction band-edge energies of semiconductor nanocrystals, ACS Nano 5 (2011) 5888–5902.
[35] L.Z. Wu, B. Chen, Z.J. Li, C.H. Tung, Enhancement of the efficiency of photocatalytic reduction of protons to hydrogen via molecular assembly, Acc. Chem. Res. 47 (2014) 2177–2185.
[36] K. Wu, Z. Chen, H. Lv, H. Zhu, C.L. Hill, T. Lian, Hole removal rate limits photodriven H_2 generation efficiency in CdS-Pt and CdSe/CdS-Pt semiconductor nanorod-metal tip heterostructures, J. Am. Chem. Soc. 136 (2014) 7708–7716.
[37] Z. Han, F. Qiu, R. Eisenberg, P.L. Holland, T.D. Krauss, Robust photogeneration of H_2 in water using semiconductor nanocrystals and a nickel catalyst, Science 338 (2012) 1321–1324.
[38] P. Kalisman, Y. Nakibli, L. Amirav, Perfect photon-to-hydrogen conversion efficiency, Nano Lett. 16 (2016) 1776–1781.
[39] Y.-J. Gao, X.-B. Li, H.-L. Wu, S.-L. Meng, X.-B. Fan, M.-Y. Huang, Q. Guo, C.-H. Tung, L.-Z. Wu, Exceptional catalytic nature of quantum dots for photocatalytic hydrogen evolution without external cocatalysts, Adv. Funct. Mater. 28 (2018) 1801769.
[40] X.-B. Han, C. Qin, X.-L. Wang, Y.-Z. Tan, X.-J. Zhao, E.-B. Wang, Bio-inspired assembly of cubane-adjustable polyoxometalate-based high-nuclear nickel clusters for visible light-driven hydrogen evolution, Appl. Catal. B: Environ. 211 (2017) 349–356.
[41] H. Li, S. Yao, H.-L. Wu, J.-Y. Qu, Z.-M. Zhang, T.-B. Lu, W. Lin, E.-B. Wang, Charge-regulated sequential adsorption of anionic catalysts and cationic photosensitizers into metal-organic frameworks enhances photocatalytic proton reduction, Appl. Catal. B: Environ. 224 (2018) 46–52.
[42] P. Huang, X.-J. Wang, J.-J. Qi, X.-L. Wang, M. Huang, H.-Y. Wu, C. Qin, Z.-M. Su, Self-assembly and photocatalytic H_2 evolution activity of two nanoscale polytantalotungstates based on unprecedented $\{Cr_3Ta_6\}$ and $\{Cr_4Ta_{12}\}$ clusters, J. Mater. Chem. A 5 (2017) 22970–22974.
[43] X.J. Kong, Z. Lin, Z.M. Zhang, T. Zhang, W. Lin, Hierarchical integration of photosensitizing metal-organic frameworks and nickel-containing polyoxometalates for efficient visible-light-driven hydrogen evolution, Angew. Chem. Int. Ed. 55 (2016) 6411–6416.
[44] B. Matt, J. Fize, J. Moussa, H. Amouri, A. Pereira, V. Artero, G. Izzet, A. Proust, Charge photo-accumulation and photocatalytic hydrogen evolution under visible light at an Iridium(III)-photosensitized polyoxotungstate, Energy Environ. Sci. 6 (2013) 1504–1508.
[45] H. Lv, J. Song, H. Zhu, Y.V. Geletii, J. Bacsa, C. Zhao, T. Lian, D.G. Musaev, C. L. Hill, Visible-light-driven hydrogen evolution from water using a noble-metal-free polyoxometalate catalyst, J. Catal. 307 (2013) 48–54.
[46] X. Liu, Y. Li, S. Peng, G. Lu, S. Li, Photocatalytic hydrogen evolution under visible light irradiation by the polyoxometalate α-$[AlSiW_{11}(H_2O)O_{39}]^{5-}$-Eosin Y system, Int. J. Hydrogen Energy 37 (2012) 12150–12157.
[47] J. Zhao, Y. Ding, J. Wei, X. Du, Y. Yu, R. Han, A molecular Keggin polyoxometalate catalyst with high efficiency for visible-light driven hydrogen evolution, Int. J. Hydrogen Energy 39 (2014) 18908–18918.
[48] W. Wu, T. Teng, X.-Y. Wu, X. Dui, L. Zhang, J. Xiong, L. Wu, C.-Z. Lu, A cobalt-based polyoxometalate catalyst for efficient visible-light-driven H_2 evolution from water splitting, Catal. Commun. 64 (2015) 44–47.
[49] G. Paille, A. Boulmier, A. Bensaid, M.H. Ha-Thi, T.T. Tran, T. Pino, J. Marrot, E. Riviere, C.H. Hendon, O. Oms, M. Gomez-Mingot, M. Fontecave, C. Mellot-Draznieks, A. Dolbecq, P. Mialane, An unprecedented $\{Ni_{14}SiW_9\}$ hybrid polyoxometalate with high photocatalytic hydrogen evolution activity, Chem. Commun. 55 (2019) 4166–4169.
[50] Y.S. Ding, H.Y. Wang, Y. Ding, Visible-light-driven hydrogen evolution using a polyoxometalate-based copper molecular catalyst, Dalton Trans. 49 (2020) 3457–3462.
[51] L. Jiao, Y. Dong, X. Xin, L. Qin, H. Lv, Facile integration of Ni-substituted polyoxometalate catalysts into mesoporous light-responsive metal-organic framework for effective photogeneration of hydrogen, Appl. Catal. B: Environ. 291 (2021) 120091–120102.
[52] L. Qin, C. Zhao, L.-Y. Yao, H. Dou, M. Zhang, J. Xie, T.-C. Weng, H. Lv, G.-Y. Yang, Efficient photogeneration of hydrogen boosted by long-lived dye-modified Ir(III) photosensitizers and polyoxometalate catalyst, CCS Chem. (2021) 651–663.
[53] T. Cui, L. Qin, F. Fu, X. Xin, H. Li, X. Fang, H. Lv, Pentadecanuclear Fe-containing polyoxometalate catalyst for visible-light-driven generation of hydrogen, Inorg. Chem. 60 (2021) 4124–4132.
[54] H.N. Kim, T.W. Kim, K.H. Choi, I.Y. Kim, Y.R. Kim, S.J. Hwang, Self-assembly of nanosized 0D clusters: CdS quantum dot-polyoxotungstate nanohybrids with strongly coupled electronic structures and visible-light-active photofunctions, Chem. Eur. J. 17 (2011) 9626–9633.
[55] X. Xing, R. Liu, X. Yu, G. Zhang, H. Cao, J. Yao, B. Ren, Z. Jiang, H. Zhao, Self-assembly of CdS quantum dots with polyoxometalate encapsulated gold nanoparticles: enhanced photocatalytic activities, J. Mater. Chem. A 1 (2013) 1488–1494.
[56] M. Wang, X. Shang, X. Yu, R. Liu, Y. Xie, H. Zhao, H. Cao, G. Zhang, Graphene-CdS quantum dots-polyoxometalate composite films for efficient photoelectrochemical water splitting and pollutant degradation, Phys. Chem. Chem. Phys. 16 (2014) 26016–26023.
[57] X.L. Zhai, J. Liu, L.Y. Hu, J.C. Bao, Y.Q. Lan, Polyoxometalate-decorated g-C_3N_4-wrapping snowflake-like CdS nanocrystal for enhanced photocatalytic hydrogen evolution, Chem. Eur. J. 24 (2018) 15930–15936.
[58] Y. Dong, Q. Han, Q. Hu, C. Xu, C. Dong, Y. Peng, Y. Ding, Y. Lan, Carbon quantum dots enriching molecular nickel polyoxometalate over CdS semiconductor for photocatalytic water splitting, Appl. Catal. B: Environ. 293 (2021) 120214–120226.
[59] H. Lv, T.P. Ruberu, V.E. Fleischauer, W.W. Brennessel, M.L. Neidig, R. Eisenberg, Catalytic light-driven generation of hydrogen from water by Iron dithiolene complexes, J. Am. Chem. Soc. 138 (2016) 11654–11663.
[60] J.M. Clemente-Juan, E. Coronado, J.R. Galan-Mascaros, C.J. Gomez-Garcia, Increasing the nuclearity of magnetic polyoxometalates. Syntheses, structures, and magnetic properties of salts of the heteropoly complexes $[Ni_3(H_2O)_3(PW_{10}O_{39})H_2O]^{7-}$, $[Ni_4(H_2O)_2(PW_9O_{34})_2]^{10-}$, and $[Ni_9(OH)_3(H_2O)_6(HPO_4)_2(PW_9O_{34})_3]^{16-}$, Inorg. Chem. 38 (1999) 55–63.
[61] H. Lv, Y. Chi, J. van Leusen, P. Kogerler, Z. Chen, J. Bacsa, Y.V. Geletii, W. Guo, T. Lian, C.L. Hill, $[\{Ni_4(OH)_3AsO_4\}_4(B\text{-}\alpha\text{-}PW_9O_{34})_4]^{28-}$: a new polyoxometalate structural family with catalytic hydrogen evolution activity, Chem. Eur. J. 21 (2015) 17363–17370.
[62] W.R. McNamara, Z. Han, P.J. Alperin, W.W. Brennessel, P.L. Holland, R. Eisenberg, A cobalt-dithiolene complex for the photocatalytic and electrocatalytic reduction of protons, J. Am. Chem. Soc. 133 (2011) 15368–15371.
[63] X. Zhou, H. Yu, D. Zhao, X. Wang, S. Zheng, Combination of polyoxotantalate and metal sulfide: a new-type noble-metal-free binary photocatalyst $Na_8Ta_6O_{19}$/$Cd_{0.7}Zn_{0.3}S$ for highly efficient visible-light-driven H_2 evolution, Appl. Catal. B: Environ. 248 (2019) 423–429.
[64] A. Madonia, M. Martin-Sabi, A. Sciortino, S. Agnello, M. Cannas, S. Ammar, F. Messina, D. Schaming, Highly efficient electron transfer in a carbon dot-polyoxometalate nanohybrid, J. Phys. Chem. Lett. 11 (2020) 4379–4384.
[65] H.-L. Li, M. Zhang, C. Lian, Z.-L. Lang, H. Lv, G.-Y. Yang, Ring-shaped polyoxometalate built by $\{Mn_4PW_9\}$ and PO_4 units for efficient visible-light-driven hydrogen, Evol. CCS Chem. 2 (2020) 2095–2103.